

Strengthening and mechanical stability mechanisms in nanostructured bainite

Behzad Avishan · Carlos Garcia-Mateo ·
Lucia Morales-Rivas · Sasan Yazdani ·
Francisca G. Caballero

Received: 10 December 2012 / Accepted: 24 April 2013 / Published online: 3 May 2013
© Springer Science+Business Media New York 2013

Abstract Understanding the main relationships between the microstructure parameters controlling the strength and ductility of low temperature bainitic microstructures is of considerable importance for further development of these grades. Although the microstructure essentially consists of solely two phases, bainitic ferrite and retained austenite, the complexity of the different microstructural characteristics, the natural consequence of its unique transformation mechanisms, might not provide with one unique answer, but a set of several parameters interdependent among them. This paper will deal with some of these relationships' microstructure properties, strength, and ductility, with special emphasis in the mechanical stability (TRIP effect) of retained austenite.

Introduction

Almost routinely, today it is possible to design alloys which give rise to a nanostructured bainite by isothermal transformation at low temperatures (125–325 °C). The development process is relatively simple and it implies the use of the detailed phase transformation theory and some metallurgical facts [1–5]. The microstructure consists of a matrix of ultrafine bainitic ferrite plates (30–40 nm) and a dispersed

second phase, retained austenite. Retained austenite exhibits two very distinguishable morphologies, as thin films between the plates of ferrite, also in the nano-range, and as blocks separating sheaves of bainite (groups of bainitic ferrite plates sharing a common crystallographic orientation). This mixed microstructure, with a strong composite character, presents an excellent balance of mechanical properties [6, 7]. Due to the absence of fine carbides, the steels have a high resistance to cleavage fracture and void formation. Regarding the strength, the main contribution mainly comes from the substructure of the ferritic matrix, i.e., high fraction of slender plates of bainitic ferrite. On the other hand, it is believed that ductility in these microstructures is controlled by the amount and nature of retained austenite [7–10], which is a ductile phase when compared with bainitic ferrite. As further improvement of ductility can be achieved by transformation to martensite, TRIP effect, retained austenite mechanical stability (or its capability to transform to martensite under strain or stress) must be controlled and understood.

In this work, an attempt is made to review and depict some of the most important relationships between different microstructural parameters and the strength and ductility of the final microstructure in a new set of nanostructured bainitic steels. Special attention will be paid to the effect that the chemical composition, morphology-size-distribution, and strength of austenite have on its mechanical stability and therefore on the evolution of the TRIP effect as a function of the applied strain.

Materials and experimental procedure

The chemical composition of the alloys used in this study is listed in Table 1, and it is the result of theoretical design by

B. Avishan · S. Yazdani
Faculty of Materials Engineering, Sahand University of
Technology, Tabriz, Iran

C. Garcia-Mateo (✉) · L. Morales-Rivas · F. G. Caballero
MATERIALIA Research Group, Department of Physical
Metallurgy, National Center for Metallurgical Research
(CENIM-CSIC), Avda. Gregorio Del Amo, 8, 28040 Madrid,
Spain
e-mail: cgm@cenim.csic.es

Table 1 Chemical composition, all in wt%

	C	Si	Mn	Ni	Mo	Cr	V	Co	Al
Steel 1	0.91	1.58	1.98	0.06	0.25	1.12	0	1.37	0.53
Steel 2	0.90	1.51	0.94	2.61	0.25	1.14	0.09	1.37	0.59

means of the phase transformation theory alone [11] in order to obtain carbide-free bainitic microstructures after isothermal heat treatment at low temperature. Further details on the steps followed to design such types of alloys are given elsewhere [3–5]. Suffice to say that both alloys were designed to have almost identical T_0 curves and bainitic region in TTT diagrams [12]. A high C content insures low bainite and martensite start temperature, B_S and M_S , while 1.5 wt% Si inhibits the precipitation of cementite [11]. Elements such as Co and Al have an accelerating effect on bainitic transformation [13], Mo avoids temper embrittlement due to P and Mn, and Cr and Ni are used for hardenability purposes. In the case of steel 2, the Mn content was reduced by almost 1 wt% and its effect on the T_0 curve as well as on the TTT diagram needed to be compensated by a substantial increase in the Ni content, 2.6 wt%. Small quantities of V were added in steel 2 to restrict prior austenite grain size (PAGS) growth during the austenitizing heat treatment by pinning grain boundaries with V(CN).

Both alloys were cast in an induction furnace under inert Ar atmosphere and were electro slag remelted to gain clean steels free of inclusions. After being homogenized at 1200 °C for 2 h, they were hot rolled at a temperature of about 950 °C. Finally, lumps of $5 \times 5 \times 10 \text{ mm}^3$ were cut and prepared for heat treatments. By means of high resolution dilatometry, the A_{c3} temperature of both alloys was determined to be ≈ 845 °C; therefore, austenitization was performed at 900 °C for 30 min. in a salt bath. Samples were then immediately transferred to another salt bath at 200 °C, a temperature between the theoretically determined M_s and B_s temperatures, 80 and 290 °C, respectively, where samples were held for 3 days, the time needed to insure the end of bainitic transformation.

Prior austenite grain size was evaluated after applying the austenitization conditions, following the thermal etching technique procedures described in Refs. [14, 15].

To reveal the microstructure, metallographic samples were cut, ground, and polished following the standard procedures. A 2 % Nital etching solution was used to reveal bainitic microstructure. Scanning electron microscopy observation was carried out on a FEG-SEM HITACHI S-4800 field emission gun scanning electron microscope (SEM-FEG) operating at 7 kV. Before etching, samples were polished using colloidal silica suspension. High magnification SEM-FEG micrographs were used to

determine the distribution and size of the different microstructural features analyzed.

TEM specimens were sliced from 3-mm-diameter rods of the heat-treated material, mechanically thinned to 0.06 mm, and then twin-jet electropolished to perforation using a mixture of 5 % perchloric acid, 25 % glycerol, and 70 % ethanol at 10 °C at 45 V. The samples were examined on a TEM JEOL 2100 transmission electron microscope operated at 200 keV.

Quantitative X-ray diffraction analysis was used to determine the fraction of retained austenite (V_γ) and its carbon content (C_γ). For this purpose, samples were machined, ground, and finally polished using 1 μm diamond paste; samples were then subjected to several cycles of etching and polishing to obtain an undeformed surface and were finally finished in colloidal silica. They were then step scanned in a Bruker-Axs D8 X-ray diffractometer using unfiltered $\text{Co K}\alpha$ radiation. The scanning speed (2θ) was less than 0.3 degree/min. The machine was operated at 40 kV and 30 mA. The volume fraction of retained austenite was calculated from the integrated intensities of (111), (200), (220), and (311) austenite peaks and those of (110), (200), and (211) planes of ferrite; using this number of peaks avoids possible bias due to crystallographic texture [16]. Moreover, the retained austenite composition was calculated making use of the relationship between the lattice parameter and chemical composition as reported in Ref. [17] and assuming that during transformation, only carbon diffuses [11]. Thus, the concentration ratios of all elements but C should be equal in the bulk material as in the retained austenite (γ); in other words, $(x_{\text{Fe}}/x_j)_{\text{bulk}} = (x_{\text{Fe}}/x_j)_\gamma$, where j denotes any substitutional element in the alloy and x_{Fe} y x_j are the concentrations of Fe and of the substitutional elements [7, 18]. The X-ray data from the undeformed microstructure were also analyzed for non-uniform strains, i.e., peak profile broadening, which is directly related to the dislocation density [19].

Tensile tests were performed at room temperature in specimens with a section of $2.9 \times 1.4 \text{ mm}^2$ and a gage length of 10 mm. All experiments were assisted by an extensometer fitted to electronic equipment that allowed the continuous tracking of load–displacement data during tests. Load and elongations measured during uniaxial tensile tests were converted to engineering and true stress–strain curves. Strain hardening was characterized by the incremental strain-hardening exponent $n = d(\ln\sigma)/d(\ln \epsilon)$ obtained from the true stress–true plastic strain curve.

Hardness was measured as HV(30 kg) and the presented results correspond to an average of at least 3 values. Finally, all the necessary thermodynamic calculations were performed by means of MTDATA with the NPL-plus database for steels [20].

Results and discussion

Microstructural characterization

Experimental quantitative data presented in Table 2 show that, as expected, the microstructure consists of a mixture of two phases, a dominant phase, bainitic ferrite (α), with fractions of 0.58 and 0.67 in steel 1 and steel 2, respectively, and carbon-enriched regions of retained austenite (γ). Bainitic ferrite in Fig. 1a, b is present as feather-like features called sheaves, which consist of aggregates of plates (or subunits) sharing a common crystallographic orientation, see darker features in Fig. 1c, d. When referring to retained austenite morphology, it is necessary to distinguish between the blocky morphology, bound by crystallographic variants of bainite sheaves and exhibiting polygonal shape in two-dimensional sections, dark blocky features in Fig. 1a, b, and the thin films of austenite found between the subunits within a given sheaf of bainite, see the interwoven lighter phase in Fig. 1c, d. Extensive TEM observation failed to reveal any cementite as it is expected from adding 1.5 wt% Si [11], see micrographs in Fig. 2. Bainitic ferrite plates show the well-known rational Kurdjumov–Sachs (K–S) orientation relationship with the parent austenite in which it grows [11, 21, 22], as illustrated in Fig. 2 with the corresponding selected area diffraction (SAD) patterns, presenting the K–S crystallographic relationship, with $\{111\}\gamma//\{110\}\alpha$ and $\langle 110 \rangle \gamma//\langle 111 \rangle \alpha$, between bainitic ferrite and austenite. TEM micrographs also revealed intense dislocation debris due to the plastic relaxation of the shape change occurring as a consequence of the displacive growth of bainite. The plastic relaxation commonly takes place via generation of both, dislocations in the austenite/bainitic ferrite interface, and also via micro/nano-twins in the austenite in contact with bainitic ferrite plates [23–25]. As the transformation temperature decreases, the combination of local increase in dislocation density caused by the yielding of the austenite together with the increase of the strength of austenite itself is found to be the main factor controlling the scale of the microstructure, both factors increasing in intensity as transformation temperature is lowered [26, 27].

Table 2 Quantitative data on microstructure at room temperature after isothermal heat treatment at 200 °C

	Fraction (± 0.03)		Fraction of		Size/nm		
	α	γ	γ films	γ blocky	α plates	γ films	γ blocks
Steel 1	0.58	0.42	0.09	0.33	39 ± 2	38 ± 2	808 ± 22
Steel 2	0.67	0.33	0.10	0.23	35 ± 1	30 ± 1	598 ± 23

Where α stands for ferrite and γ for retained austenite, the fraction of retained as thin films or blocks was calculated as described in the main text [28]

Both grades were conceived under those premises, and bainitic ferrite plate thickness in Table 2 comes to corroborate the benefits of low transformation temperatures on the scale of the final microstructure, with thicknesses within the nano-range, 39 and 35 nm for steel 1 and 2, respectively, and a distribution, Fig. 3, that does not show noticeable differences between both alloys. Slenderness is not exclusive of bainitic ferrite; retained austenite trapped between the plates of ferrite, thin films as those shown in Figs. 1c, d and 2, has an average size of 38 and 30 nm for both steels, Table 2. Consistently, distribution of thin film sizes for steel 2, Fig. 4, is narrower than that of steel 1. Bigger differences arise in terms of the austenite block size and distribution between both microstructures, Table 2. Steel 1 has revealed an average block size of $\sim 0.8 \mu\text{m}$ and a prominent tail toward higher values, some features as big as those pointed out in Fig. 1, $\sim 2 \mu\text{m}$, in contrast with steel 2 where the measured average thickness was $\sim 0.6 \mu\text{m}$ and the distribution narrower, Fig. 4. It has been rationalized that about 15 % of the volume contained within the boundaries of a bainite sheaf consists of retained austenite films interspersed with bainitic ferrite subunits [28]. Hence, the fraction of the film and blocky retained austenite can be deduced from the total, see Table 2. In the present work, retained austenite as thin films is present in both steels almost in the same quantity, 10 %, while steel 1 contains about 10 % more of blocky austenite than steel 2.

The smaller and narrower distribution of retained austenite in steel 2 as compared with steel 1 is coherent with the PAGS measurements, 37 ± 1 and $20 \pm 1 \mu\text{m}$ for steel 1 and 2, respectively. In steel 2, at the austenitization T, V(CN) precipitates are expected to exert control on the PAGS by pinning of the grain boundaries [20, 29]; it has to be noted though that such precipitates were not sought or observed in TEM.

Table 3 shows the retained austenite chemical composition derived from the lattice parameter obtained from the X-ray and following the procedure formerly described. Results thus obtained indicate that there are no differences in composition between retained austenite in steel 1 and steel 2 other than those inherent to their bulk chemical composition, i.e., Mn, Ni, and V content. The C enrichment of retained austenite is a natural consequence of bainite transformation mechanisms; once bainite stops growing, the excess of C trapped within diffuses to the parent austenite. Moreover, it should be highlighted that X-ray is a “bulk” analysis in the sense that C content estimation by means of this technique is an average of regions of the material that may contain carbon-enriched regions such as dislocations and phase interfaces, which are very distinctive features of this type of microstructure [30]. Therefore, this technique is unable to disclose the large variation of austenite C content from region to region. It has been

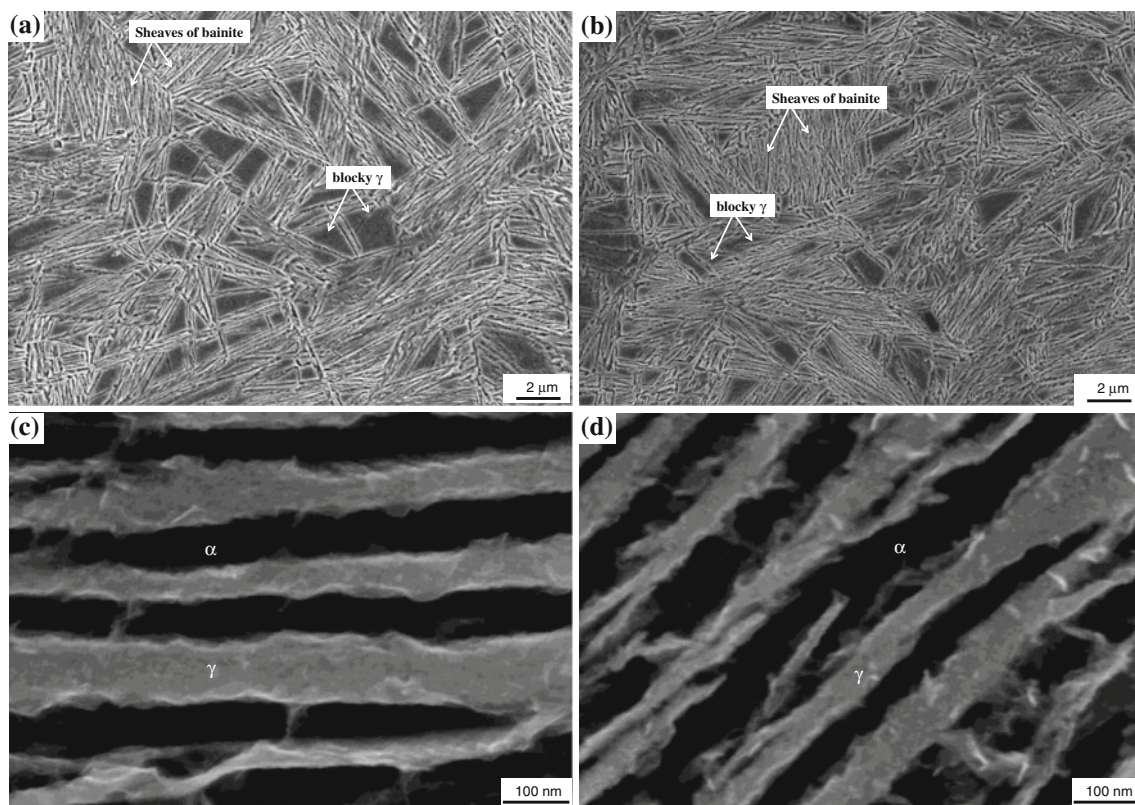


Fig. 1 Scanning electron micrographs of the microstructure revealed at room temperature after isothermal heat treatment at 200 °C for steel 1 **a, c**, and for steel 2 **b, d**

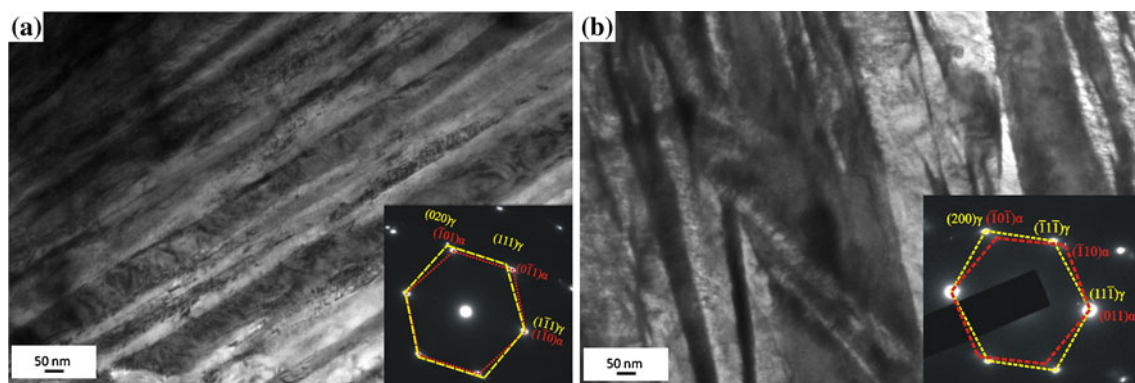


Fig. 2 TEM micrographs of the microstructure revealed at room temperature after isothermal heat treatment at 200 °C for **a** steel 1 and **b** for steel 2. Also embedded, the SAD pattern

proved that in bainitic microstructures of the type shown in this work, C in austenite is distributed inhomogeneously, where thin films of retained austenite trapped between bainite plates can host C in much higher quantities than the blocks trapped between the sheaves of bainite [18, 31–33].

As previously indicated, an indirect measurement of the dislocation density can be derived from microstrain

measurement, broadening in the X-ray diffraction peaks. The dislocation density value thus obtained for bainitic ferrite (ρ_{α}) in both steels is $\sim 1.1 \times 10^{16} \text{ m}^{-2}$. In the case of retained austenite, the measured microstrain differences resulted in dislocation densities, ρ_{γ} , of 6.9×10^{15} and $9.0 \times 10^{15} \text{ m}^{-2}$ for steel 1 and 2, respectively. The results are consistent with the formation of a higher fraction of bainitic ferrite in steel 2 as compared with steel 1. Note that

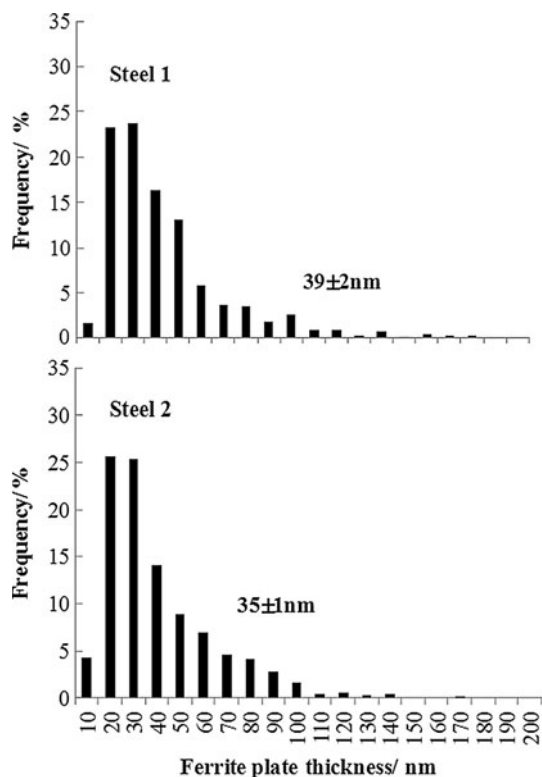
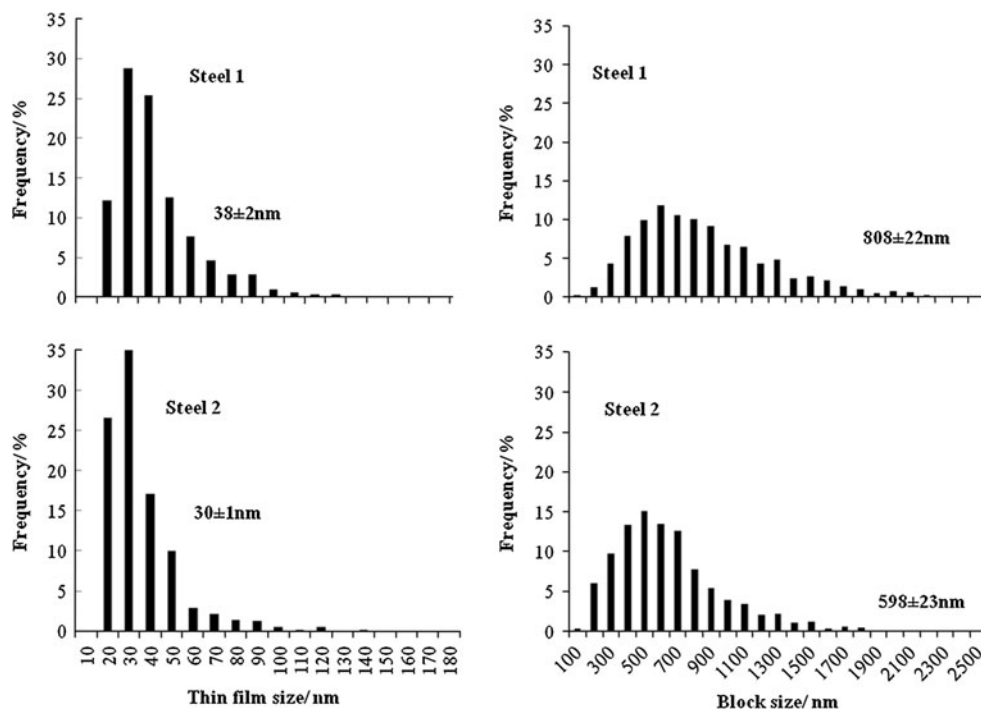


Fig. 3 Distribution of bainitic ferrite plate thicknesses and its corresponding average size

those dislocation density values are in good agreement with those previously reported for similar microstructures [6, 34].

Fig. 4 Distribution and corresponding average sizes of retained austenite films and blocks



Mechanical behavior

Typical strain–stress curves from tensile tests at room temperature are presented in Fig. 5. The curves are characterized by continuous yielding, as expected from microstructures containing unlocked dislocations introduced by the plastic accommodation of the shape change. Although there is evidence that ferrite retains an excess concentration of carbon, even after annealing, a majority of dislocations are believed to be mobile. The gradual yielding behavior sometimes persists after stress-relief heat treatments. There are a variety of obstacles to dislocation motion, (solute atoms, boundaries, thin films of retained austenite), each with a different ability to obstruct plastic deformation. Many of the obstacles are not uniformly distributed, so obstacle-free areas will exist into which dislocations can penetrate at low stresses, thus giving rise to a gradual deviation from elastic deformation. Another scale of heterogeneity can arise when a representative fraction of softer phase is included in the microstructure such as retained austenite. Plastic deformation at first focuses in the softer phase; the hard phase only begins to deform when the softer phase has strain hardened sufficiently to transfer load, leading to continuous yielding.

Table 4 contains a summary of the mechanical properties obtained for both steels, showing remarkable levels of strength, with yield strengths (YS) ranging from 1.4 to 1.7 GPa and ultimate tensile strengths (UTS) of about 2.1 GPa. Strength can be rationalized if we keep in mind that there are several operative strengthening mechanisms

Table 3 Retained austenite chemical composition in wt%, calculated as described in Ref. [18]

	C	Si	Mn	Ni	Mo	Cr	V	Co	Al	$\Delta G^{\gamma/\alpha}/\text{J mol}^{-1}$
Steel 1	1.01	1.58	2.02	0.05	0.24	1.12	0	1.36	0.52	−2629
Steel 2	1.07	1.50	0.93	2.60	0.24	1.14	0.08	1.36	0.58	−2283

$\Delta G^{\gamma/\alpha}$ represents the chemical free energy change for transformation of austenite to martensite with no change in chemical composition

that may contribute to the strength of ferrite: (a) size of the bainitic ferrite plates—the thinner they are, the shorter the mean free path for dislocation glide is, leading to the enhancement of the strength; (b) dislocation density; and (c) carbon in solid solution within ferrite. But, in this context, it has been known that bainitic ferrite is supersaturated with an excess of carbon [32]. This carbon fails to partition the residual austenite in spite of the fact that the process is not limited by atomic mobility [35] or even in spite of prolonged heat treatment [31, 32, 36–38]. An interpretation of these observations partially attributed the reluctance of the carbon to partition to the presence of dislocations which trap the solute. However, recent work has shown conclusively using the atom-probe technique that large quantities of excess carbon may also remain in defect-free solid solution [39, 40]. Therefore, there may be a contribution of C in both solid solution and, through its effect, on the mobility of dislocations.

Usually, the well-known Hall–Petch relation is used to describe the microstructure size contribution to strength of coarse-grained microstructures, since it relies on the existence of sufficient space on a slip plane to build a pileup of dislocations. In low temperature bainite, it has been shown that growth happens in the form of very fine plates. The mean free path through these plates is only about twice the thickness of the plate. Dislocation pileups cannot therefore form and the Hall–Petch relation ceases to apply. Instead, yielding involves the spread of dislocations which are present in the plate boundaries, between pinning points, until the resulting loop hits the perimeter of the plate. When the energetics of this process is considered [41, 42], the grain size strengthening becomes $\Delta\sigma \approx 115 L^{-1}$ where $L \approx 2t$ is the mean linear intercept measured in μm and $\Delta\sigma$ in MPa. From dislocation density, the contribution is given by $\Delta\sigma \approx 7.34 \times 10^{-6} \rho^{0.5}$ [43], where ρ is in m^{-2} and $\Delta\sigma$ in MPa. Keeping in mind that steel 1 contains less bainitic ferrite than steel 2, the contribution to the strength of the microstructure arising from the plate thickness is estimated to be 855 and 1100 MPa, respectively, while from the dislocation density, it is much lower, i.e., 446 and 515 MPa, respectively.

So far, all the strength contributions analyzed correspond to ferrite, which is the strongest and dominant phase. Therefore, it is difficult to assess the retained austenite contribution to strength in these microstructures.

Qualitatively, retained austenite interlath films can increase the strength by transforming to martensite during testing by the TRIP effect.

The levels of ductility accompanying such high strength values are quite reasonable, ϵ_T of 7.7 and 14 % for steel 1 and 2, respectively. In this sense, it is evident from Fig. 5 and Table 4 that plastic deformation is uniformly distributed along the gage length of the samples, showing little or no necking; in other words, most or all of the total elongation achieved is uniform elongation. This behavior is also visible in the incremental work-hardening curves, “n” versus strain in Fig. 5, where in the case of steel 1, there is a continuous increase toward the instability criteria, straight line, which is never reached; all the elongation is uniform. In the case of the steel 2, after a rapid increase, there is a more progressive evolution up to necking. Surprisingly and contrary to the common trend, in steel 2, it has been possible to get an increase of ductility without sacrificing strength. In this sense, most of the published data on ductility of bainitic steels point out retained austenite as the microstructural feature controlling ductility [7–9]. This is because austenite, being an fcc structure, has a large number of slip planes, i.e., has a higher ductility and strain-hardening rate than ferrite (bcc) [44, 45], harder phase [46], and it would be expected to enhance ductility as far as austenite is homogeneously distributed between plate boundaries (film austenite), contributing to suppress crack and/or void initiation at the grain boundaries. However, isolated pools of austenite (blocky austenite) would influence unfavorably both elongation and strength because of the strain localization in these areas [28]. There is also the possibility to enhance ductility via the TRIP effect, i.e., strain-induced transformation of retained austenite to martensite. The transformation implies a relaxation of the local stress concentration and extra strain hardening by means of the progressive increase in volume fraction of a hard phase and also by additional plastic deformation due to transformation strains.

The mechanical stability of retained austenite, i.e., its ability to transform to martensite under strain, is a concept that has to be handled carefully. In alloys containing austenite of low mechanical stability, the strain-induced transformation occurs in early stages of deformation, resulting in little or null benefit of the strain hardening related to deterring plastic instability or necking in the later

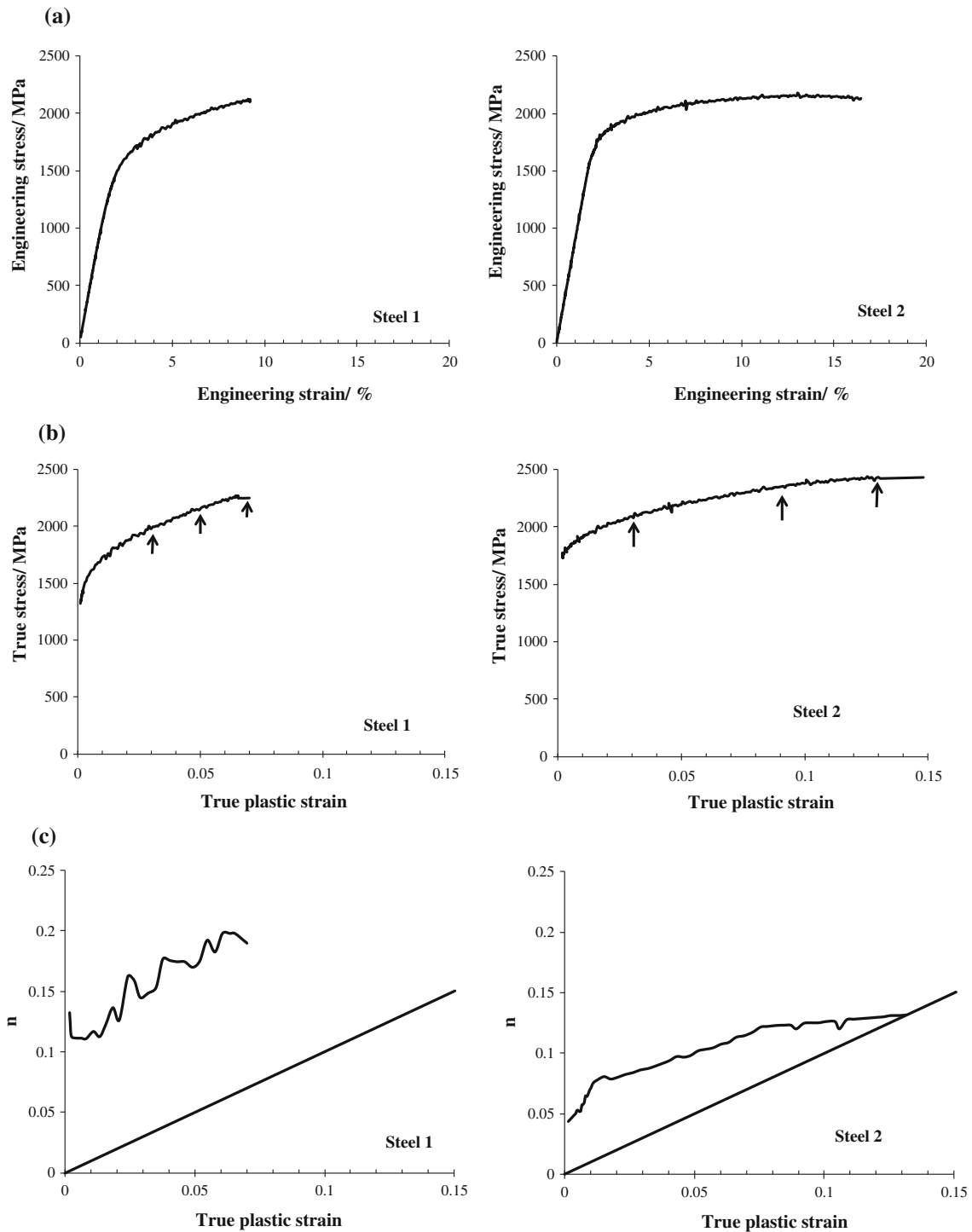


Fig. 5 Engineering and true tensile strain–stress curves of steel 1 and steel 2, and the corresponding incremental work-hardening exponent, n . Straight line represents the instability criterion, i.e., $\epsilon_p = n$. Arrows indicate at which strains the interrupted tensile tests were performed

stages of deformation. On the other hand, if austenite becomes mechanically more stable and transforms at higher strains, the associated strain hardening effectively increases resistance to necking and fracture. However, if austenite is too stable, the presence of large amounts of

austenite at necking (instability criterion) does not guarantee an effective TRIP effect. So, the strain-induced transformation will enhance ductility if retained austenite is moderately stable against straining. There is a correlation between the shape of the incremental work-hardening

Table 4 Tensile test results

	YS/MPa	UTS/MPa	$\varepsilon_w/\%$	$\varepsilon_T/\%$	HV
Steel 1	1405 ± 30	2115 ± 30	7.7 ± 2	7.7 ± 2	530 ± 10
Steel 2	1730 ± 40	2182 ± 50	10.5 ± 2	14.0 ± 2	561 ± 10

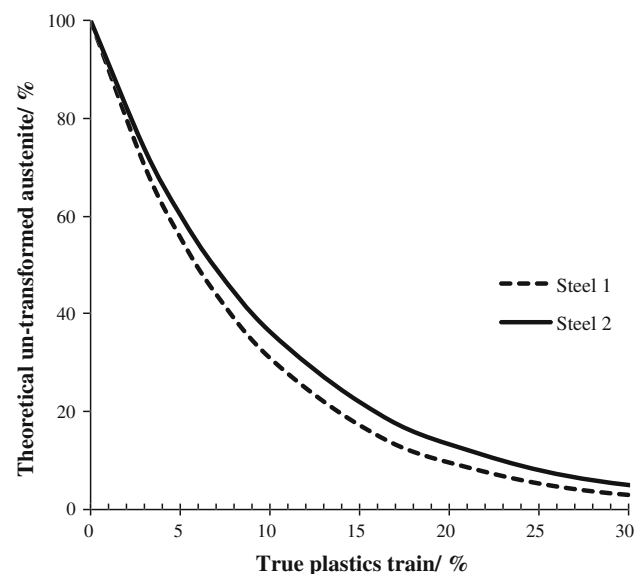
exponent “n” versus strain curve, Fig. 5, and the rate at which retained austenite transforms to martensite [7–9, 47]; an interpretation of curves in Fig. 5 could be as follows: In the case of steel 1, there is a rapid transformation of austenite into martensite at early stages, and it is not possible to get the full advantage of the augmentation of ductility consequence of the austenite–martensite transformation. But, in the case of steel 2, the same transformation proceeds progressively until the instability criterion is reached and the increment in strain hardening thus obtained enhances ductility. In an attempt to correlate the TRIP effect evolution with the ductility behavior, interrupted tensile tests were performed at the strain levels indicated by arrows in Fig. 5, and then the evolution of retained austenite fraction was analyzed by means of X-ray. Understanding the main parameters that control the austenite–martensite transformation is of considerable importance in order to obtain detailed knowledge of the ductility behavior of these microstructures, i.e., TRIP effect evolution.

Among those parameters controlling the mechanical stability, the chemical composition of retained austenite is known to play an important role. Elements such as C, Mo, Ni, and Mn [48, 49] significantly enhance the austenite mechanical stability; from C to Mn, the element influence diminishes. The calculated chemical driving force at room temperature for the transformation of austenite into martensite $\Delta G^{\alpha\gamma}$ (i.e., ferrite of the same chemical composition) [20], see Table 3, implies that steel 1 is slightly more prone to such transformation than steel 2; in other words, and attending exclusively to the chemical composition, retained austenite in steel 2 is mechanically more stable than that of steel 1. A more intuitive way of presenting such results is by means of the Sherif et al. [50] model, based on a quantitative theory for the strain-induced transformation of retained austenite in a class of TRIP-assisted steels. The model allows the progress of austenite transformation to be followed as a function of the plastic strain, chemical composition, and the temperature at which the deformation is carried out. The effect of the latter two variables is expressed through the chemical driving force for transformation, which has been introduced into a simple equation for strain-induced transformation, $\ln V_\gamma - \ln V_\gamma^0 = k_1 \Delta G^{\alpha\gamma} \varepsilon$, where V_γ^0 and V_γ represent the initial austenite fraction and the remaining fraction, after transformation-induced plasticity, respectively, ε is the plastic strain, and k_1 is a constant. The model can adequately be used for assessing the austenite

mechanical stability in a wide range of TRIP-aided steel and its applicability to bainitic steel has been demonstrated, see for example [8, 51]. Theoretical calculations of such type are presented in Fig. 6, demonstrating that indeed the rate of strain-assisted transformation from austenite to martensite is slightly superior in steel 1 than in steel 2 despite its higher V_γ^0 . As the calculations only account for retained austenite chemical composition, through its influence in the value $\Delta G^{\alpha\gamma}$, the described differences can only be justified in terms of the differences in Ni and Mn shown in Table 3 and their depicted influence in austenite mechanical stability.

Attending to the experimental results regarding the strain evolution of retained austenite fraction, Fig. 7, it is clear that at first in steel 1, the rate of transformation is superior to that of steel 2 indeed, but there is a point where the TRIP effect does not evolve and almost 70 % of the retained austenite remains in the microstructure just before failure. On the other hand, for steel 2, transformation progresses during deformation up to much higher strain levels and only 25 % of the retained austenite remains. Therefore, it is safe to insure then that chemical composition of retained austenite itself does not explain the ductility behavior.

Morphology-size-distribution of retained austenite is a trio playing an important role on its mechanical stability [23, 52–54]. Particle size of the retained austenite is a crucial stabilization factor and it has been suggested that the grain size of austenite should be in the range of 0.01–1 μm to insure TRIP effect [55]. Larger retained austenite is unstable and transforms quickly to martensite at small strains, while grains smaller than 0.01 μm might be too stable to undergo the strain-induced transformation

**Fig. 6** Theoretical evolution of untransformed retained austenite as a function of strain

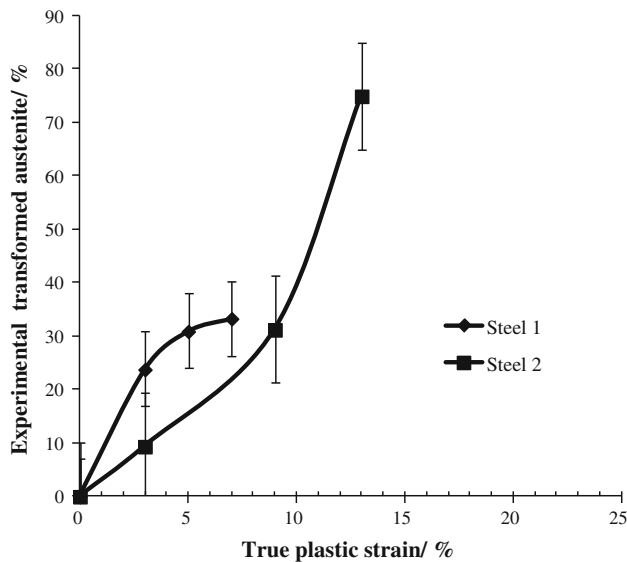


Fig. 7 Experimental evolution of transformed retained austenite as a function of strain

[56, 57], and the reasons are described as follows. It should be kept in mind that smaller grains of austenite are subjected to a high constrain to transformation exerted by the surrounding matrix (plates of bainitic ferrite). Naturally thin films of retained austenite contain lower potential nucleation sites for the transformation of martensite and, as a consequence, require higher driving force for its nucleation. Finally, as already described, there is a strong correlation between the size of the retained austenite and its C content, showing a higher level of C supersaturation, a strong stabilizer element, as its size decreases.

Detailed observation of X-ray profiles at the different strains, as the $(200)_\gamma$ in Fig. 8, also reveals that the austenite lattice parameter tends to increase as deformation increases, which is linked with the fact that austenite with lower C content transforms first to martensite, mechanically less stable, the remaining austenite being richer in C, and therefore having a bigger lattice parameter. The intensity of the austenite peaks also decreases as deformation increases, i.e., austenite transforms to martensite. In the case of steel 1, shifting of the peak is evident from $\varepsilon = 0$ to 3 %; as nearly no austenite–martensite transformation takes place from $\varepsilon = 3$ –7 %, the peaks are nearly indistinguishable in terms of height (fraction of austenite) and 2θ position (C content). On the other hand, for steel 2, the evolution of the intensity and position of the peak are quite evident as the strain increases; the fraction of austenite decreases and its C content increases.

For steel 1, with more austenite and bigger blocks than steel 2, Fig. 4, up to $\varepsilon = 3$ %, 10 % of retained austenite transforms to martensite and the C content only changes from 1.01 to 1.17 wt%, a clear indication that there is a

representative fraction of low C austenite blocks (unstable) that might be transforming, as for example those big blocks detailed in Fig. 1. Contrarily, for steel 2 with less of those big blocks and a narrower distribution and smaller average size of the same, at $\varepsilon = 3$ %, only 4 % of retained austenite transforms and the C content increases from 1.07 to 1.25 wt%, evidencing the existence of a small fraction of very poor in C austenites that transform at the beginning.

This is supported if we apply a simple level rule, $C_\gamma = V_{\gamma f} C_f + V_{\gamma b} C_b$, where the subscripts f and b stand for thin film and block, respectively, and C and V for the carbon content, just mentioned, and fraction of each morphology, respectively, see Table 2. To simplify the calculation, it is reasonable to assume that up to $\varepsilon = 3$ %, only the blocks will transform, the thin films remain stable, and their average C content (C_f) can be fixed in approx. 7.41 at% [18]. Calculations thus performed reveal that although in steel 1 the blocky austenite seems to be richer than in steel 2, 0.6 versus 0.4 wt%, the transformation that has taken place up to $\varepsilon = 3$ % leaves a C_b of 0.65 and 0.6 wt% in steel 1 and 2, respectively, which can only be explained by the existence of a small fraction of very low C_b in the case of steel 2 and a representative fraction of not that low in C_b austenite blocks in the case of steel 1.

In this sense, heterogeneities in the microstructure that lead to effective variations of the austenite stability are known as favorable for spreading the effect of the transformation all along straining and for postponing localization [2, 58, 59]. But, it does not seem to be the case in the present study where steel 1 with wider distribution of retained austenite reaches a deformation where the transformation of austenite–martensite halts, while in steel 2, with smaller and narrower distribution of austenite, the transformation carries on up to necking.

Distribution of retained austenite is directly linked to the existing amount as it has been proved that the formation of strain-induced martensite, vital to reach acceptable ductility properties, can only be tolerated if the austenite maintains a uniform and percolated structure through the material [51, 60], the latter in the form of films constituting an interconnected network. It has been shown that below ~ 10 % of retained austenite, the interconnection is lost leading to the failure of the tensile specimen. Apparently, in steel 2, total elongation is reached with a fraction of retained austenite that is very close to this percolation threshold, 8 %, while in steel 1, the specimen breaks down when austenite is approximately 30 %, well above the defined threshold.

So far, none of the described parameters controlling the stability of retained austenite, chemical composition, and morphology-size-distribution seem to explain why in steel 1 there is a halt of the transformation, while in steel 2, with more stable austenite and a less favorable distribution of sizes, the transformation carries on up to necking.

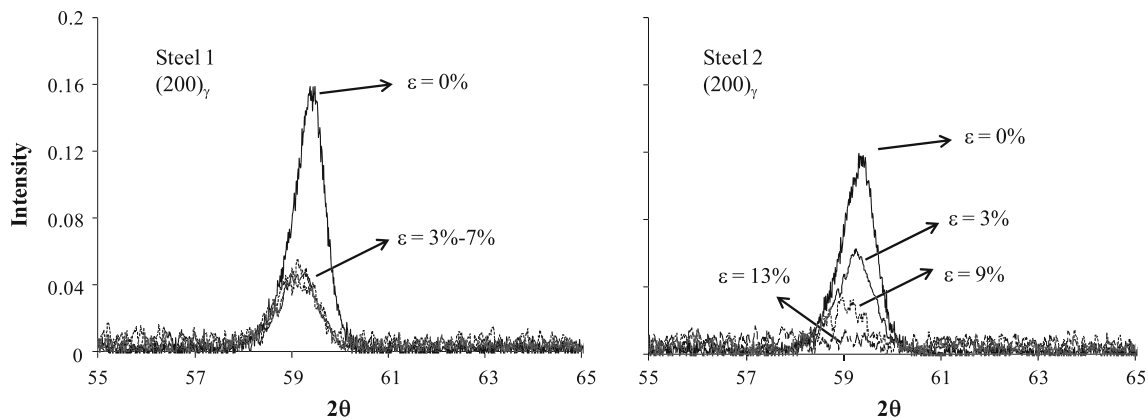


Fig. 8 X-ray $(200)_\gamma$ peak profile evolution as a function of strain

The reason could be found if it is kept in mind that austenite–martensite transformation takes place when the corresponding chemical free energy change accompanying transformation is equal to or larger than the energy necessary to overcome the resistance to volume deformation, strain energy, and the creation of new surfaces which accompany the transformation. The resistance of austenite to plastic deformation is considered to contribute to the magnitude of this non-mechanical free energy term and can delay or even halt martensitic transformation [61, 62]. In similar terms, the matrix might be playing an important role in the stability and efficiency of TRIP effect [58, 63–66]; a very strong surrounding matrix could also impede the motion of glissile interfaces necessary for the coordinated movement of atoms, which accompanies the austenite–martensite transformation. Therefore, less transformation is expected when austenite and the surrounding matrix are stronger. In this sense, elements such as Mn and Ni, both present in different quantities in steel 1 and 2, are known for strengthening capacity in solid solution; when compared to Ni, Mn by far is the element with the strongest influence [43, 67, 68], both in austenite and ferrite. Bainitic ferrite in steel 1 is also expected to contain higher C content than steel 2; C is the strongest solid solution strengthener. For all those reasons, it is speculated that the high strength of austenite and the ferritic matrix where it is contained, might be the reasons for the complete stabilization of retained austenite after $\varepsilon = 3\%$ in the case of steel 1.

Conclusions

Two nanostructured bainitic microstructures have been investigated in terms of the strength and ductility relationships with the various microstructural features that characterize these microstructures. Strength has been shown to be controlled by the amount and scale of the bainitic ferrite matrix. The study of the ductility is

invariably linked to the evolution of the TRIP effect, i.e., the mechanical stability of retained austenite.

Retained austenite microstructural parameters, such as chemical composition, morphology-size-distribution, and strength have been analyzed trying to elucidate which role they were playing on controlling its mechanical stability. According to the results, the strength of austenite itself might be an important factor limiting or even halting the TRIP effect, dramatically limiting the ductility of the microstructure.

Acknowledgements The authors acknowledge E. Urones-Garrote from the Centro de Microscopia y Citometría (UCM) for assistance with the TEM. C. García-Mateo and F.G. Caballero would like to thank the Spanish Ministry of Economy and Competitiveness Plan Nacional de I + D+I (2008-2011) for supporting their research under the auspices of the National Project MAT2010-15330. L. Morales-Rivas also acknowledges the same Ministry for financial support in the form of a PhD Research Grant (FPI). Behzad Avishan acknowledges the Iranian Science Ministry for the provision of a Grant for a short-term stay in CENIM.

References

1. Caballero FG, Santofimia MJ, Capdevila C, García-Mateo C, De García Andrés C (2006) Design of advanced bainitic steels by optimisation of TTT diagrams and T₀ curves. *ISIJ Int* 46(10):1479
2. Garcia-Mateo C, Caballero FG, Sourmail T, Kuntz M, Cornide J, Smanio V, Elvira R (2012) Tensile behaviour of a nanocrystalline bainitic steel containing 3 wt% silicon. *Mater Sci Eng A* 549:185
3. Garcia-Mateo C, Caballero FG, Bhadeshia HKDH (2003) Development of hard bainite. *ISIJ Int* 43(8):1238
4. Garcia-Mateo C, Caballero FG (2007) Design of carbide-free low-temperature ultra high strength bainitic steels. *Int J Mater Res* 98(2):137
5. Garcia-Mateo C, Caballero FG, Sourmail T, Smanio V and Garcia de Andres C (2012) Composition Design of nanocrystalline bainitic steels by diffusionless solid reaction: theoretical calculations. Submitted to *ISIJ Int* for its evaluation
6. Garcia-Mateo C, Caballero FG (2005) Ultra-high-strength bainitic steels. *ISIJ Int* 45(11):1736
7. Garcia-Mateo C, Caballero FG (2005) The role of retained austenite on tensile properties of steels with bainitic microstructures. *Mater Trans JIM* 46(8):1839

8. Caballero FG, García-Mateo C, Chao J, Santofimia MJ, Capdevila C, De Andrés CG (2008) Effects of morphology and stability of retained austenite on the ductility of TRIP-aided bainitic steels. *ISIJ Int* 48(9):1256
9. Garcia-Mateo C, Caballero FG, Chao J, Capdevila C, Garcia De Andres C (2009) Mechanical stability of retained austenite during plastic deformation of super high strength carbide free bainitic steels. *J Mater Sci* 44(17):4617. doi:10.1007/s10853-009-3704-4
10. Sandvik BPJ, Navalainen HP (1981) Structure-property relationships in commercial low-alloy bainitic-austenitic steel with high strength, ductility, and toughness. *Met Technol* 8(pt 6):213
11. Bhadeshia HKDH (2001) Bainite in steels. transformations, microstructure and properties, 2nd edn. Institute of Materials, Minerals and Mining, London
12. Bhadeshia HKDH (1982) Thermodynamic analysis of isothermal transformation diagrams. *Met Sci Heat Treat* 16(3):159
13. Garcia-Mateo C, Caballero FG, Bhadeshia HKDH (2003) Acceleration of low-temperature bainite. *ISIJ Int* 43(11):1821
14. de Andres CG, Bartolome MJ, Capdevila C, Martin DS, Caballero FG, Lopez V (2001) Metallographic techniques for the determination of the austenite grain size in medium-carbon microalloyed steels. *Mater Charact* 46(5):389
15. de Andres CG, Caballero FG, Capdevila C, San Martin D (2002) Revealing austenite grain boundaries by thermal etching: advantages and disadvantages. *Mater Charact* 49(2):121
16. Dickson MJ (1969) Significance of texture parameters in phase analysis by X-ray diffraction. *J Appl Crystallogr* 2:176
17. Dyson DJ, Holmes B (1970) Effect of alloying additions on lattice parameter of austenite. *J Iron Steel Inst* 208:469
18. Garcia-Mateo C, Caballero FG, Miller MK, Jimenez JA (2012) On measurement of carbon content in retained austenite in a nanostructured bainitic steel. *J Mater Sci* 47(2):1004. doi:10.1007/s10853-011-5880-2
19. Williamson GK, Smallman RE (1956) III. Dislocation densities in some annealed and cold-worked metals from measurements on the X-ray Debye-Scherrer spectrum. *Philos Mag* 1(1):34
20. MTDATA (2004) Phase diagram calculation software. National Physical Laboratory, Teddington
21. Bhadeshia HKDH, Christian JW (1990) Bainite in steels. *Metall Trans A* 21 A(4):767
22. Furuhashi T, Kawata H, Morito S, Maki T (2006) Crystallography of upper bainite in Fe–Ni–C alloys. *Mater Sci Eng A* 431(1–2):228
23. Bhadeshia HKDH, Edmonds DV (1979) The bainite transformation in a silicon steel. *Metall Trans A* 10(7):895
24. Chang LC, Bhadeshia HKDH (1995) Metallographic observations of bainite transformation mechanism. *Mater Sci Technol* 11(2):105
25. Caballero FG, Yen HW, Miller MK, Yang JR, Cornide J, Garcia-Mateo C (2011) Complementary use of transmission electron microscopy and atom probe tomography for the examination of plastic accommodation in nanocrystalline bainitic steels. *Acta Mater* 59(15):6117
26. Singh SB, Bhadeshia HKDH (1998) Estimation of bainite plate-thickness in low-alloy steels. *Mater Sci Eng A* 245(1):72
27. Cornide J, Garcia-Mateo C, Capdevila C, Caballero FG (2012) An assessment of the contributing factors to the nanoscale structural refinement of advanced bainitic steels. *J Alloys Compd.* doi:10.1016/j.jallcom.2011.11.066
28. Bhadeshia HKDH, Edmonds DV (1983) Bainite in silicon steels: new composition-property approach. Part I. *Met Sci Heat Treat* 17(9):411
29. Gladman T (1997) The physical metallurgy of microalloyed steels. Institute of Materials, London
30. Caballero FG, Miller MK, Babu SS, Garcia-Mateo C (2007) Atomic scale observations of bainite transformation in a high carbon high silicon steel. *Acta Mater* 55(1):381
31. Caballero FG, Garcia-Mateo C, Santofimia MJ, Miller MK, García de Andrés C (2009) New experimental evidence on the incomplete transformation phenomenon in steel. *Acta Mater* 57(1):8
32. Bhadeshia HKDH, Waugh AR (1982) Bainite: an atom-probe study of the incomplete reaction phenomenon. *Acta Metall* 30(4):775
33. Stone HJ, Peet MJ, Bhadeshia HKDH, Withers PJ, Babu SS, Specht ED (2008) Synchrotron X-ray studies of austenite and bainitic ferrite. *Proc R Soc Lond Ser A* 464(2092):1009
34. Garcia-Mateo C, Caballero FG, Capdevila C, Andres CGd (2009) Estimation of dislocation density in bainitic microstructures using high-resolution dilatometry. *Scr Mater* 61(9):855
35. Bhadeshia HKDH (1987) Bainite in Steels. Paper presented at the Phase transformations '87
36. Peet M, Babu SS, Miller MK, Bhadeshia H (2004) Three-dimensional atom probe analysis of carbon distribution in low-temperature bainite. *Scr Mater* 50(10):1277
37. Garcia-Mateo C, Peet M, Caballero FG, Bhadeshia HKDH (2004) Tempering of hard mixture of bainitic ferrite and austenite. *Mater Sci Technol* 20(7):814
38. Caballero F, Miller M, Clarke A, Garcia-Mateo C (2010) Examination of carbon partitioning into austenite during tempering of bainite. *Scr Mater* 63(4):442
39. Caballero FG, Miller MK, Garcia-Mateo C, Cornide J, Santofimia MJ (2012) Temperature dependence of carbon supersaturation of ferrite in bainitic steels. *Scr Mater* 67(10):846
40. Caballero FG, Miller MK, Garcia-Mateo C, Cornide J (2012) New experimental evidence of the diffusionless transformation nature of bainite. *J Alloys Compd.* doi:10.1016/j.jallcom.2012.02.130
41. Langford G, Cohen M (1969) Strain hardening of iron by severe plastic deformation. *ASM-Trans* 62:623
42. Langford G, Cohen M (1970) Calculation of cell-size strengthening of wire-drawn iron. *Metall Mater Trans A* 1(5):1478
43. Bhadeshia HKDH, Honeycombe RWK (2006) Steels: microstructure and properties. Butterworths-Heinemann (Elsevier), Amsterdam
44. Olofsson J, Larsson D, Svensson IL (2011) Effect of Austempering on Plastic Behavior of Some Austempered Ductile Iron Alloys. *Metall Mater Trans A* 42(13):3999
45. Yang J, Putunda SK (2004) Influence of a novel two-step austempering process on the strain-hardening behavior of austempered ductile cast iron (ADI). *Mater Sci Eng A* 382(1–2):265
46. Lan HF, Liu XH, Du LX (2011) Ultra-hard bainitic steels processed through low temperature heat treatment. *Adv Mater Res* 156–157:1708
47. Sugimoto K, Kobayashi M, Hashimoto S (1992) Ductility and strain-induced transformation in a high-strength transformation-induced plasticity-aided dual-phase steel. *Metall Trans A* 23 A(11):3085
48. Kirk D, Payne J (1999) Transformation induced in austenitic stainless steels by shot peening. Paper presented at the ICSP7: 7th International Conference on Shot Peening Warsaw (Poland), 29 Sept 1
49. Nohara K, Ono Y, Ohashi N (1977) Composition and grain size dependence of strain induced martensitic transformation in metastable austenitic stainless steels. *Tetsu To Hagane-J ISIJ* 63(5):212
50. Sherif MY, Garcia-Mateo C, Sourmail T, Bhadeshia HKDH (2004) Stability of retained austenite in TRIP-assisted steels. *Mater Sci Technol* 20(3):319
51. Sherif MY (2006) Characterisation and development of nanostructured, ultrahigh strength, and ductile bainitic steels. Ph.D., University of Cambridge. Available online at <http://www.msm.cam.ac.uk/phase-trans/2000/phd.html>

52. Zackay VF, Parker ER, Fahr D, Busch R (1967) Enhancement of ductility in high-strength steels. *ASM Trans* 60(2):252
53. K-i Sugimoto, Misu M, Kobayashi M, Shirasawa H (1993) Effects of second phase morphology on retained austenite morphology and tensile properties in a TRIP-aided dual-phase steel sheet. *ISIJ Int* 33(7):775
54. Seol J-B, Raabe D, Choi P-P, Im Y-R, Park C-G (2012) Atomic scale effects of alloying, partitioning, solute drag and austempering on the mechanical properties of high-carbon bainitic-austenitic TRIP steels. *Acta Mater* 60(17):6183
55. Wang J, Van der Zwaag S (2001) Stabilization mechanisms of retained austenite in transformation-induced plasticity steel. *Metall Mater Trans A* 32(6):1527
56. Lanzillotto CAN, Pickering FB (1982) Structure property relationships in dual-phase steels. *Met Sci Heat Treat* 16(8):371
57. Balliger NK, Gladman T (1981) Work hardening of dual-phase steels. *Met Sci Heat Treat* 15(3):95
58. Lani F, Furnemont Q, Van Rompaey T, Delannay F, Jacques PJ, Pardoën T (2007) Multiscale mechanics of TRIP-assisted multiphase steels: II Micromechanical modelling. *Acta Mater* 55(11):3695
59. Hase K, Garcia-Mateo C, Bhadeshia HKDH (2006) Bimodal size-distribution of bainite plates. *Mater Sci Eng A* 438–440:145
60. Bhadeshia HKDH (2010) Nanostructured bainite. *Proc R Soc Lond Ser A* 466(2113):3
61. Nichol TJ, Judd G, Ansell GS (1977) The relationship between austenite strength and the transformation to martensite in Fe-10 pct Ni-0.6 pct C alloys. *Metall Trans A* 8(12):1877
62. Breinan EM, Ansell GS (1970) The influence of austenite strength upon the austenite-martensite transformation in alloy steels. *Metall Trans A* 1(6):1513
63. Ryu JH, Kim D-I, Kim HS, Bhadeshia HKDH, Suh D-W (2010) Strain partitioning and mechanical stability of retained austenite. *Scr Mater* 63(3):297
64. Hojo T, Sugimoto KI, Mukai Y, Ikeda S (2008) Effects of aluminium on delayed fracture properties of ultra high strength low alloy TRIP-aided steels. *ISIJ Int* 48(6):824
65. Jacques PJ, Ladrière J, Delannay F (2001) On the influence of interactions between phases on the mechanical stability of retained austenite in transformation-induced plasticity multiphase steels. *Metall Mater Trans A* 32(11):2759
66. Timokhina IB, Hodgson PD, Pereloma EV (2004) Effect of microstructure on the stability of retained austenite in transformation-induced-plasticity steels. *Metall Mater Trans A* 35 A(8):2331
67. Peet MJ (2001) Modelling the hot-deformation of austenite. M. Phil., University of Cambridge
68. Zajac S, Komenda J, Morris P, Dierickx P, Matera S, Peñalba Diaz F (2005) Quantitative structure-property relationships for complex bainitic microstructures. Ref 7210-PR/247